frontiers | Frontiers in Neuroscience

TYPE Perspective
PUBLISHED 05 January 2026
DOI 10.3389/fnins.2025.1725728

OPEN ACCESS

EDITED BY
Amir Shmuel,
McGill University, Canada

REVIEWED BY
Alberto Del Guerra,
University of Pisa, Italy

*CORRESPONDENCE
Cláudia Régio Brambilla
✉ c.regio.brambilla@fz-juelich.de

RECEIVED 15 October 2025
REVISED 21 November 2025
ACCEPTED 01 December 2025
PUBLISHED 05 January 2026

CITATION
Brambilla CR, Hilgers J, Khalid U, Anasovi N, Kikacheishvili T, Mauler J, Choi C-H, Scheins JJ, Shah NJ and Lerche CW (2026) Future prospects for image-derived input function in molecular imaging quantification with the 7 T MR-BrainPET insert. *Front. Neurosci.* 19:1725728. doi: 10.3389/fnins.2025.1725728

Future prospects for image-derived input function in molecular imaging quantification with the 7 T MR-BrainPET insert

Cláudia Régio Brambilla[1]*, Julia Hilgers[1], Usman Khalid[1], Ninea Anasovi[2], Tornike Kikacheishvili[3], Jörg Mauler[1], Chang-Hoon Choi[1], Jürgen J. Scheins[1], N. Jon Shah[1,4,5,6] and Christoph W. Lerche[1]

[1]Medical Imaging Physics, Institute of Neuroscience and Medicine 4, INM-4, Forschungszentrum Jülich GmbH, Jülich, Germany, [2]Engineering, Agricultural University of Georgia, Tbilisi, Georgia, [3]Informatics and Engineering School, Georgian American University, Tbilisi, Georgia, [4]Department of Neurology, RWTH Aachen University, Aachen, Germany, [5]Institute of Neuroscience and Medicine 11, INM-11, Forschungszentrum Jülich GmbH, Jülich, Germany, [6]JARA-BRAIN, Aachen, Germany

Positron emission tomography (PET) and magnetic resonance imaging (MRI) offer complementary information about the human brain in health and disease. The simultaneous 7 T MR-BrainPET insert enables molecular imaging quantification beyond the current limits. Here we present the current status of the field highlighting PET/MR synergies for the image-derived input function (IDIF). We also discuss promising applications that will benefit from these advancements, as well the challenges to be addressed in the near future.

KEYWORDS

UHF 7 T MR, BrainPET 7 T insert, molecular imaging, neuroimaging, image-derived input function, PET quantification

1 Introduction

In vivo neuroimaging techniques have progressed significantly in recent decades, advancing understanding of neural processes in health and disease (Jones et al., 2012; Fink and Schneider, 2007). A major step toward simultaneous multimodal imaging was achieved with the combination of PET and MRI (Schlemmer et al., 2008), and has been continuously developed since (Herzog and Lerche, 2016). While MRI enables precise access to neuroanatomy, flow dynamics and several other functional mappings, its sensitivity is insufficient for molecular imaging, which studies the biodistribution of molecular targets and metabolic processes *in vivo*. Compared to MRI, PET has a million-fold higher detection sensitivity and is, therefore, the most important, non-invasive molecular imaging modality. The pico-molar detection sensitivity of PET enables imaging of neurotransmitter/receptor concentrations, and potentially allows the evaluation of endogenous neurotransmitter fluctuations—stimulated by pharmacologic or cognitive challenges (Kegeles and Mann, 1997). Most brain-PET scans are performed with whole-body scanners, which requires trade-offs in the image performance. Therefore, several brain-dedicated scanners have been developed (Caldeira et al., 2019; Catana, 2019; Li et al., 2024).

Brain-dedicated PET scanners are adapted to brain geometry, with reduced ring diameter (solid angle coverage) and thicker scintillation crystals leading to a better sensitivity and smaller scintillation crystals leading to a better spatial resolution. High detection sensitivity and time resolution are needed for a good image signal-to-noise ratio (SNR), quantification

precision, and allow short acquisition intervals in the case of dynamic studies. The high spatial resolution of brain-PET scanners enables reliable region delineation and minimizes the partial volume effect (PVE) for the human cortex. As the cortex is highly folded, the spatial resolution should, ideally, be homogeneous over the entire field-of-view (FOV). Another important advantage of improved image-derived input function (IDIF) performance is it avoids the need for arterial cannulation, as the internal carotid arteries (ICAs) can be resolved in the PET image and used as input for the full quantification with kinetic modeling (Figure 1; Volpi et al., 2024). In addition, temporal resolution is very important, since for IDIF the whole-blood curves can be sampled with shorter image frames to better estimate its peak (<2–5 s; Kang et al., 2025; Volpi et al., 2023).

Despite the advantages of brain-dedicated PET scanners, a disadvantage is the increased parallax error whenever the scintillation detectors are not prepared to estimate the depth of interaction (DOI) of the γ-photons (Lerche et al., 2018). Additionally, care has to be taken to implement adequate data corrections to minimize motion effects, γ-photon attenuation, and scattering to assure high quantification fidelity.

2 Instrumentation innovations in MR and brain PET imaging

Compared to conventional field strengths (1.5 and 3 T), 7 T MRI offers increased SNR and specificity (Feinberg et al., 2023). This enables imaging with both higher spatial and temporal resolutions, allowing for better characterization of subtle and prominent anatomical features and microvascular structures. The benefits of 7 T (Springer et al., 2016; De Cocker et al., 2018; Feng et al., 2022; Koning et al., 2015; Zhu et al., 2016) have been demonstrated in various applications, with the focus here on the brain and the ICA imaging.

Accessing superior visualization of tiny intracranial branches, e.g., vessel walls, enables more specific assessment of properties, such as wall thickening and other subtle vascular characteristics that are hardly identifiable at lower fields, leading to more accurate images. To provide a comprehensive characterization of the vessel wall, modified turbo spin-echo (van der Kolk et al., 2013; Blankena et al., 2016; Zhu et al., 2018; Kleinloog et al., 2014) and time-of-flight (TOF; Park et al., 2018; Cosottini et al., 2024; von Morze et al., 2007), contrast-enhanced (Osuafor et al., 2022; Harteveld et al., 2015) and phase-contrast (Kang et al., 2016). MR angiography techniques are frequently employed.

One possible method for visualizing the ICA without using a contrast agent is TOF MR angiography (TOF-MRA), which provides precise localization information on the arterial inflow. TOF-MRA at 7 T has been shown to improve contrast-to-noise ratio (CNR) and thus visualization of cerebral arteries compared to 3 T (von Morze et al., 2007; Dimitrakopoulou-Strauss et al., 2021). This offers the possibility for higher resolution TOF-MRA with more precise delineation of the ICA lumen, enabling more accurate correction of the PVE and segmentation of the PET images to improve the IDIF estimation in MR-driven techniques.

A common challenge in cross-calibrating IDIF data to bolus injections and blood sampling is correcting for dispersion due to varying flow velocities across the vessel cross-section and course (Dimitrakopoulou-Strauss et al., 2021).

The advanced speed-accelerated 4D flow sequence (Schmitter et al., 2020) provides valuable haemodynamic information within the ICAs that improves our understanding of cerebrovascular disease progression. However, (B_1^+) inhomogeneity can be a challenge, but using a robust, large-dynamic-range parallel-transmit mapping technique to enable B_1-shimming enhanced ICA image quality (de Buck et al., 2024). Furthermore, the introduction of artificial intelligence (AI)-driven models has advanced vascular imaging data analysis, enabling precise vessel identification and localization (Banerjee et al., 2024), and supporting an automated workflow that reduces reliance on inconsistent MRA data.

Despite the advantages afforded by 7 T MRI, the higher field strength increases the susceptibility to artifacts caused by arterial and cerebrospinal fluid (CSF) pulsation (Seginer et al., 2024), which reduces the accurate delineation of the vessel volume due to signal loss, ghosting artifacts and blurring. To minimize these artifacts, cardiac gating and motion compensation techniques can be used (Kuo et al., 2019).

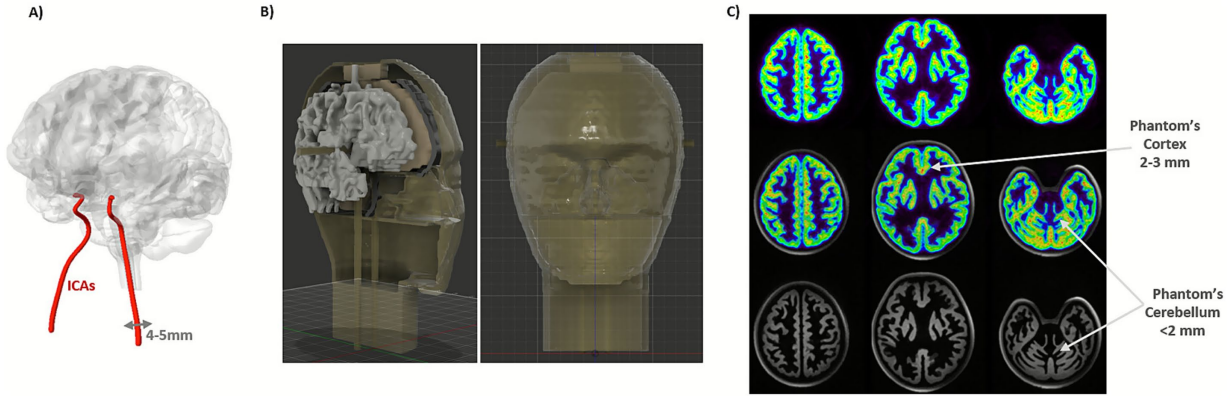

FIGURE 1
(A) Schematic visualization of the brain and ICAs. **(B)** Designed anthropomorphic head phantom with ICAs (updated from phantom shown in **C**). **(C)** Head phantom (Iida et al., 2013) acquisition in the 7 T MR-BrainPET showing the cortex and cerebellar structures in contrast with the human head from Figure 2A bottom (upper: BrainPET 7 T image, middle: PET/MR fused image and bottom: 7 T MR MP2RAGE T_1-weighted image).

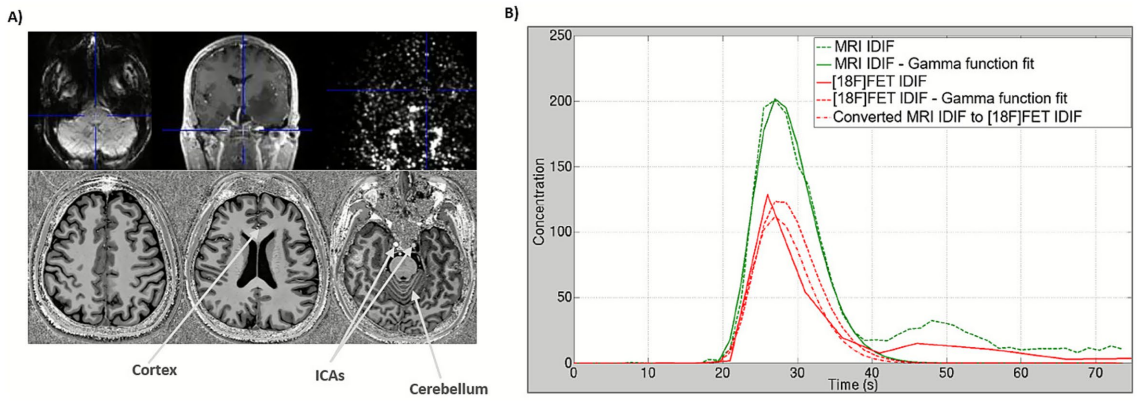

FIGURE 2
(A) Upper row from left to right: transaxial contrast-enhanced EPIK image, coronal MPRAGE T_1-weighted structural image at 3 T MR showing the structure of the ICAs with contrast, and coronal [^{18}F]FET 4th frame with 5 s. Bottom: transaxial MP2RAGE T_1-weighted structural image at 7 T MR clearly showing the structure of the ICAs, cortex, and cerebellum without contrast agents. **(B)** Plots with IDIF curves from each modality with Gamma function fits and conversion from MRI IDIF to PET IDIF (estimated with 3 T MR-BrainPET upper images in **A**). Figure adapted from Caldeira et al. (2015).

Several projects are developing simultaneous PET/MR imaging at 7 T, aiming for full MR compatibility, significantly increased spatial resolution (1-2 mm), and increased sensitivity compared to standard clinical PET scanners (Allen et al., 2024; Won et al., 2021; Lerche et al., 2023). To achieve high spatial resolution across the entire PET FOV, the aforementioned scanners use DOI-capable scintillation detectors, which reduce parallax errors.

The cortex and ICA are of interest in neuroscientific applications, with average thicknesses or internal diameters of 2-5 mm and 4-5 mm, respectively (Baz et al., 2021). A noticeable PVE occurs in these structures when they are smaller than twice the spatial resolution of the system (Hoffman et al., 1979), requiring a spatial resolution around 1-2 mm to minimize this. On the other hand, increased detection sensitivity enhances image SNR, reducing statistical errors in the PET quantitative measurements, e.g., the rate constants required for compartment kinetic modeling (Dahlbom et al., 2005). Additionally, higher SNR enables shorter image frames for denser sampling of the radiotracer's vascular phase, crucial for IDIF, which lasts ~90 s. Currently available PET scanners only allow very coarse sampling, resulting in an inaccurate determination of the bolus activity concentration, leading to error propagation during quantification. Reducing the sampling interval (currently ~15 s), while simultaneously increasing the SNR, would significantly reduce these errors. The PET image SNR can also be improved by taking TOF information into account during image reconstruction, and coincidence resolving time (CRT) has improved considerably to 200 ps in recent years. The BrainPET 7 T insert developed at the Forschungszentrum Jülich (FZJ) achieves a spatial resolution of 1.6 mm, a sensitivity of 11%, and a CRT of 620 ± 6 ps (Niekämper et al., 2025). This corresponds to a 2–3 times better resolution and is more than double the sensitivity of the BrainPET 3 T insert (Caldeira et al., 2019). At the same time, the BrainPET 7 T achieves a detection rate for the noise equivalent counts that is ~10 times higher than that of the BrainPET 3 T. Similar values are expected with the Human Dynamic NeuroChemical Connectome (HDNCC) scanner (Allen et al., 2024). However, due to the use of DOI-capable scintillation detectors, the two 7 T inserts under development have poorer CRT.

2.1 Brain PET in image quantification

For over 15 years, scientists at FZJ have advanced PET/MR brain imaging using one of only four prototype hybrid commercial 3 T MR-BrainPET inserts available worldwide (Herzog et al., 2011). Multiple tracers, including [^{18}F]FDG, [^{18}F]FET, [^{15}O]H_2O, have been employed alongside diverse MR sequences in clinical studies (Caldeira et al., 2019; Rajkumar et al., 2021; Mauler et al., 2024; Zhang et al., 2014; Mauler et al., 2020; Régio Brambilla et al., 2022).

In the context of IDIF, studies have applied semi-automatic ICA segmentation, PVC, new reconstruction methods, and dual simultaneous PET/MR acquisitions (Caldeira et al., 2015; da Silva et al., 2015; Anasovi et al., 2024). Most recently, AI has been applied in our studies for segmentation (Hilgers et al., 2025). In a pilot study with retrospective [^{15}O]H_2O data (Zhang et al., 2014), we achieved a volume of distribution (V_T) agreement of $R^2 = 0.95$ and 0.98 in gray matter (GM) and white matter (WM), when compared to V_T using arterial input function (AIF). However, microparameters showed quantification biases of 6.5–10.5%.

The feasibility of combined and individual IDIF derivation from both, simultaneously acquired PET and MR data has already been demonstrated by extracting IDIF curves from 3 T MR EPIK (Yun et al., 2013) images with Gd-DTPA contrast and BrainPET images with [^{18}F]FET (Figure 2), as well as by evaluating the relationships between the fit parameters obtained with both modalities (Caldeira et al., 2015). The shape (two parameters) and amplitudes (one parameter) of both curves in Figure 2 display linear relationships with agreements of $R^2 = 0.86$, $R^2 = 0.98$ and $R^2 = 0.92$, respectively. Using these relationships, a conversion between the MRI and PET IDIF curves can be achieved, and a considerable potentiation of the joint determination can be expected at higher field strength (7 T vs. 3 T) and the improved imaging performance of the BrainPET 7 T component (spatial resolution 1.6 mm vs. 2 to 6 mm and sensitivity of 11% vs. 7%; Kolb et al., 2012).

Methodologically, enhancing PET/MR performance will be a vital addition to current IDIF approaches. These approaches have demonstrated that ICAs-based IDIFs—augmented by standardized PVC, motion correction, and small sets of blood samples for residual

corrections—can approach arterial-line performance for many radiotracers. In addition, PET quantification can be further improved by using MR data from 7 T for automatic carotid segmentation, PVC, and refined estimation of IDIF (Caldeira et al., 2015).

2.2 Vessel segmentation and partial volume effects

The segmentation task of small vessel diameters like ICAs in brain PET images is currently challenging because of their diameter, which may lie at the limit of the spatial resolution of most PET scanners (~3–5 mm), their tortuous shape, and pulsation. Therefore, small intracranial vessels have traditionally been segmented manually or semi-automatically, but this may change in the light of the new scanners. Methods such as k-means (Liptrot et al., 2004), soft-decision similar component analysis (Brankov et al., 2003), local mean analysis (Maroy et al., 2008), region-growing (Galovic et al., 2021) and others have already been validated (Sundar et al., 2019; Naganawa et al., 2005; Chavan et al., 2024) for a limited number of tracers.

The U-Net topology is a widely used convolutional neural network for biomedical image segmentation (Ronneberger et al., 2015), with the newer version, nnU-Net, demonstrating excellent accuracy with Dice Coefficients up to 0.97 when segmenting blood vessels (Zhu et al., 2022).

In our pilot studies for estimating the IDIF using images acquired from the 3 T MR-BrainPET insert, the U-Net model achieved a Dice coefficient of 0.82, while the nnU-Net model achieved a Dice coefficient of 0.64 compared to the manually segmented reference. The PVE, resulting from the small ICA structure and limited PET scanner resolution, leads to activity spill-out (signal loss in ICA) and spill-in from neighboring tissues, leading to systematic absolute quantification errors in the IDIF estimations compared to the AIF. Several methods have been implemented for PVC, reducing the need for blood samples or estimating a recovery coefficient based on the vessel volume and scanner resolution (Silvestri et al., 2022; de Salvi Souza et al., 2025). Options include arterialized or venous samples when equilibrium occurs during the acquisition (Galovic et al., 2021; van der Weijden et al., 2023).

Combining superior MR images with higher native contrast (TOF-MRA), without contrast agents, alongside improved PET performance, would enhance PET quantification overall. Higher-quality images would reduce or eliminate the need for extensive pre-processing, increase segmentation accuracy (e.g., minimize tissue fraction effects due to limited sampling), and ultimately speed up and streamline the research pipeline.

We believe that with this synergy, it could be possible to exceed a Dice score of 0.90 with the U-Net and nnU-Net architectures and, moreover, establish a robust IDIF estimation.

2.3 Reconstruction

Apart from hardware improvements and data corrections, image reconstruction algorithms significantly impact final image quality and quantification accuracy. In this regard, the BrainPET 7 T insert poses a challenge due to the number of LORs (5×10^9), which is addressed by the multi-layer DOI detectors. Here, the PET Reconstruction Software Toolkit (PRESTO) is ideally suited to deal with the inherent trade-off between accuracy and numerical effort in iterative reconstruction by applying scanner-independent, adaptive projection data (Scheins et al., 2011) in combination with speed-optimized projectors (Scheins et al., 2015). As a further asset, PRESTO supports Maximum-aposteriori (MAP) reconstruction using prior knowledge. In future work, specific vessel delineation, as provided by MR, could be exploited to minimize PVE. In terms of data correction accuracy, PET requires the estimation of background from Compton scattering, which can easily exceed 30% of the total statistics in neuro applications. Meanwhile, Monte Carlo simulations become feasible (Scheins et al., 2021) in dynamic imaging, potentially replacing Single Scatter Simulation, which is known to have limited accuracy and some pitfalls (Ma et al., 2020).

2.4 Multi-tracer applications

Multi-tracer imaging represents a promising advancement for assessing multiple physiological processes in a single scan session. By leveraging high-resolution PET systems and optimized signal processing algorithms, this approach can separate overlapping tracer signals, reducing patient burden and scan time compared to traditional protocols. For instance, studies have demonstrated the feasibility of triple-tracer imaging using synthetic data from clinical datasets (Hu et al., 2025).

Emerging technologies, such as those incorporating prompt gamma detection using ML-EM reconstruction methods, further enable precise multi-tracer imaging for studying complex brain disorders (Pfaehler et al., 2024). However, in multi-tracer brain PET, the IDIF faces challenges, as the overlapping signals complicate the accurate extraction of individual TACs essential for kinetic modeling. That being said, advanced signal decomposition techniques can potentially isolate tracer-specific contributions from vascular regions. Recent updates on IDIF methods highlight their non-invasive potential for human brain PET studies, noting that while ICA-based IDIF is viable for single tracers like $[^{15}O]H_2O$ and $[^{18}F]$FDG, extensions to multi-tracer scenarios will face new challenges to account for PVE, metabolite corrections (Volpi et al., 2023) and to minimize mixing effects in vascular structures (Vestergaard et al., 2021).

2.5 Phantoms for validation of IDIF estimation

Despite advances in IDIF, robust validation remains a critical challenge, particularly due to PVE (Zanotti-Fregonara et al., 2009). Dynamic phantoms incorporating realistic arterial structures and flow simulation are essential for validation. However, although most commercial head phantoms are designed for static anatomical simulation, attenuation correction, and lack dynamic flow, some prototypes simulate large vessels or modular flow-tube phantoms to systematically study IDIF recovery (Driscoll et al., 2022). Nevertheless, no commercially available dynamic head phantom with ICAs currently exists. To address this gap, we have recently developed a CT-derived, 3D printed prototype based on an existing head phantom (Iida et al., 2013). The phantom contains different fillable compartments (GM and WM), with incorporated ICAs that allow

dynamic flow simulation through the phantom during PET/MR acquisitions. Additionally, we designed a cylindrical geometric phantom with an ICA insert (Ramnarine et al., 1998) as a reliable platform for IDIF validation.

Looking ahead, further improvements are envisioned, especially with the 7 T MR-BrainPET insert. Advanced 3D printing and multi-material techniques now allow more complex, accurate geometries and realistic flow simulations, leading to more reliable IDIF-based quantification (Liaw and Guvendiren, 2017).

3 Remaining challenges

3.1 Motion

Head motion during PET imaging can lead to image blurring, artifacts, and inaccurate quantification of tracer uptake and distribution. This degrades spatial resolution, reduces signal intensity in high-uptake regions, e.g., the brain cortex, and introduces bias in kinetic modeling (Spangler-Bickell et al., 2022). Common effects include motion-induced bias in binding potential estimates and overall reduced image quality, which is particularly problematic in dynamic scans lasting usually 30–90 min, where involuntary shifts from discomfort or neurological symptoms are common (Montgomery et al., 2006). To mitigate this, various correction strategies have been developed (Spangler-Bickell et al., 2022; Iwao et al., 2022; Wang et al., 2024; Chiu et al., 2025; Chen et al., 2021; Zeng et al., 2023; Ullisch et al., 2012).

The advent of next-generation systems amplifies the necessity for robust motion correction to preserve the benefits of enhanced sensitivity and spatial resolution. This correction is indispensable, because these scanners are inherently more sensitive to head displacements (~2 mm and 1^0), which can obliterate the improved contrast and quantitative accuracy promised by such technology. This perspective underscores the shift toward real-time, data-driven corrections to support advanced applications for accurate quantification in research and clinical applications.

Despite these advancements, implementing effective head motion correction presents notable challenges, including the need for precise real-time tracking, which can be computationally intensive and susceptible to artifacts from rapid or complex head movements. For the systems described previously, integrating motion data with reconstruction algorithms should take into account the DOI effects, attenuation map mismatches and TOF precision, but signal degradation in low-count scenarios or interference from patient-specific factors (e.g., Parkinson) compromise quantification accuracy. Additionally, in hybrid PET/MR, aligning motion correction across modalities adds layers of complexity, requiring synergistic strategies.

3.2 Radiometabolites

Radiometabolite correction in brain PET applications is essential for accurate quantification, as radiolabelled metabolites can contaminate the IDIF derived from vascular regions, leading to overestimation of tracer uptake and biased kinetic parameters. Unlike invasive arterial sampling, which allows direct metabolite analysis, e.g., via radio high-performance liquid chromatography (radio-HPLC), IDIF relies on PET image data, where metabolites contribute to the total signal without differentiation, exacerbating issues in dynamic studies of neurotransmitters. The current status of the field reflects limited widespread adoption, with IDIF successfully implemented for only a minority of tracers (Table 1) due to challenges like PVE and inter-subject metabolic variability; however, recent advances include blood-free modeling approaches for early-phase tracer dynamics to estimate parameters with non-invasive kinetic modeling (Maccioni et al., 2024; Asch et al., 2025). Looking ahead, challenges persist in achieving reliable metabolite separation without blood samples for the majority of tracers.

In a multi-tracer approach, overlapping signals and complex metabolite profiles amplify the challenges. Precise blood sample analysis is needed to separate the contributions of each tracer and their metabolites. However, traditional methods like radio-HPLC are cumbersome and time-intensive when dealing with multiple compounds, potentially introducing errors from incomplete separation or variable metabolism rates across tracers. In IDIF methods, these issues are exacerbated by the inability to distinguish tracer-specific metabolites directly from vascular regions, leading to biased quantification in brain regions and reduced reliability for dynamic studies. Future techniques may address these hurdles with advanced imaging reconstruction and signal processing, enabling separation of multi-tracer signals into the ICAs dynamic imaging. Chromatographic methods, such as radio-HPLC with automated detection (including tracer signal separation), could enable real-time separation of tracers and metabolites in a few (arterialized/venous) samples taken at later time points during multi-tracer PET, providing individualized IDIF with less manual processing and invasiveness. These approaches, combined with new brain-dedicated PET systems, could streamline multi-tracer protocols, enhance quantitative accuracy, and facilitate broader adoption in research.

4 Discussion

In summary, the evolution of brain PET scanners represents a transformative leap in simultaneous multimodal neuroimaging, offering unprecedented spatial resolution, high sensitivity and temporal precision that synergize with 7 T MR techniques. These advancements address longstanding limitations in PET quantification, particularly through enhanced IDIF methods that minimize invasive arterial sampling while improving accuracy in capturing the radiotracer bolus peak and reducing PVE in vascular structures.

From a broader perspective, IDIF in brain PET quantification is poised to become closer to a standard non-invasive tool as next-generation systems close gaps in resolution and sensitivity. By integrating AI-driven segmentation, advanced reconstruction algorithms with improved correction methods, and dynamic phantoms for validation, IDIF can evolve from a tracer-specific to a multi-tracer studies. This shift reduces patient burden and unlocks new possibilities for studying the brain, such as mapping multiple dynamic neurotransmitter systems, elucidating subtle pathologies in neurodegenerative disorders and tracking psychiatric conditions. In translational medicine, IDIF-enabled

TABLE 1 List of radiotracers with IDIF validation methods depicted by imaging systems, IDIF region estimation, technique for blood sampling and metabolite's correction when applicable.

Radiotracer	Reference	System	IDIF Region	Metabolites	Technique
[^{11}C]PIB	Lopresti BJ et al. (2005) J Nucl Med.	ECAT HR + PET	ICAs	Yes	AIF; HPLC
[^{18}F]FLT	Backes H et al. (2009) J Nucl Med.	ECAT EXACT HR PET	ICAs	Yes	AIF; average metabolite correction
[^{18}F]FDG	Zanotti-Fregonara P et al. (2009) J Cereb Blood Flow Metab.	ECAT HR+ PET	ICAs	No	AIF; blood calibration
[^{18}F]FDG	Sundar LK et al. (2019) J Cereb Blood Flow Metab.	Siemens Biograph mMR PET/MRI	ICAs	No	AIF
[^{15}O]H_2O	Vestergaard MB et al. (2021) Neuroimage.	Siemens Biograph mMR PET/MRI	ICAs	No	AIF
[^{18}F]GE-179	Galovic M et al. (2021) NeuroImage.	GE SIGNA PET/MRI	ICAs	Yes	5 venous samples; HPLC
[^{18}F]FDG	Silvestri E et al. (2022) IEEE EMBC.	GE SIGNA PET/MRI	ICAs, superior sagittal sinus	No	No blood
[^{18}F]MC225	Salvi de Souza G et al. (2025) Front. Nucl. Med.	uEXPLORER Total-Body PET	Aortic arch, ICAs	Yes	AIF; HPLC
[^{18}F]FDG [^{18}F]SynVesT-1 [^{18}F] Flubatine [^{11}C]LSN3172176 [^{11}C]PHNO	Volpi T et al. (2025) J Nucl Med.	NeuroEXPLORER	ICAs, common carotid (CC)	Yes	AIF; HPLC

PET/MR could accelerate drug development by providing biomarker-driven endpoints for clinical trials, support personalized therapies for brain tumors or epilepsy, and enhance early diagnostics with multimodal data integration. However, realizing this potential requires overcoming residual challenges such as motion artifacts, radiometabolite corrections, and standardizations. Collaborative, interdisciplinary efforts are therefore needed to propel the field toward validated, blood-free, full-brain quantification.

Data availability statement

The data analyzed in this study is subject to the following licenses/restrictions: data protection rules. Requests to access these datasets should be directed to c.lerche@fz-juelich.de.

Ethics statement

The studies involving humans were approved by ethics committee of the university hospital of RWTH Aachen University and the German radiation protection law. Written informed consent for participation was obtained from the participants (results from retrospective data were reported in this work). The studies were conducted in accordance with the local legislation and institutional requirements.

Author contributions

CRB: Conceptualization, Investigation, Methodology, Project administration, Visualization, Data curation, Writing - original draft, Writing – review & editing. JH: Data curation, Formal analysis, Investigation, Methodology, Writing – review & editing. UK: Investigation, Methodology, Validation, Writing – review & editing. NA: Formal analysis, Methodology, Writing – review & editing. TK: Formal analysis, Methodology, Writing – review & editing. JM: Writing – review & editing. C-HC: Writing – review & editing. JS: Writing – review & editing. NJS: Writing – review & editing. CL: Funding acquisition, Supervision, Writing – review & editing.

Funding

The author(s) declared that financial support was received for this work and/or its publication. This work was supported by Horizon EIC 2022 Pathfinder Open, 01-RETIMAGER, Project ID: 101099096. Open access publication funded by the Deutsche Forschungsgemeinschaft (DFG, German Research Foundation), 491111487.

Acknowledgments

The authors would like to acknowledge their gratitude to Claire Rick for proofreading the manuscript.

Conflict of interest

The author(s) declared that this work was conducted in the absence of any commercial or financial relationships that could be construed as a potential conflict of interest.

Generative AI statement

The author(s) declared that Generative AI was not used in the creation of this manuscript.

Any alternative text (alt text) provided alongside figures in this article has been generated by Frontiers with the support of artificial intelligence and reasonable efforts have been made to ensure accuracy, including review by the authors wherever possible. If you identify any issues, please contact us.

Publisher's note

All claims expressed in this article are solely those of the authors and do not necessarily represent those of their affiliated organizations, or those of the publisher, the editors and the reviewers. Any product that may be evaluated in this article, or claim that may be made by its manufacturer, is not guaranteed or endorsed by the publisher.

References

Allen, MS, Byars, L, Rauscher, L, Schmidt, FP, Scipioni, M, Puryear, M, et al., editors. "Coincidence timing performance optimization of the detector for the human dynamic NeuroChemical connectome scanner." *2024 IEEE nuclear science symposium (NSS), medical imaging conference (MIC) and room temperature semiconductor detector conference (RTSD)*; (2024).

Allen, M. S., Scipioni, M., and Catana, C. (2024). New horizons in brain PET instrumentation. *PET Clinics.* 19, 25–36. doi: 10.1016/j.cpet.2023.08.001

Anasovi, N., Castro, C., Scheins, J., Tellman, L., Lohmann, P., Herzog, H., et al. (2024). Fully automated estimation of the image-derived input function in PET/MR and dedicated PET studies. EMIM 2024. Porto, Portugal. Available online at: https://e-smi.eu/wp-content/uploads/EMIM_2024_Programme_Book_for_Download_POSTERS_only.pdf.

Asch, R. H., Naganawa, M., Moisieienko, K., Weed, M., Kapinos, M., Zheng, M. Q., et al. (2025). Venous blood sampling for less invasive in vivo quantification of synaptic density with constant infusion of [(18)F]SynVesT-1 and PET. *EJNMMI Res.* 15:8. doi: 10.1186/s13550-025-01200-2

Backes, H., Ullrich, R., Neumaier, B., Kracht, L., Wienhard, K., and Jacobs, A. H. (2009). Noninvasive quantification of 18F-FLT human brain PET for the assessment of tumour proliferation in patients with high-grade glioma. *European Journal of Nuclear Medicine and Molecular Imaging.* 36, 1960–1967.

Banerjee, S., Nysjö, F., Toumpanakis, D., Dhara, A. K., Wikström, J., and Strand, R. (2024). Streamlining neuroradiology workflow with AI for improved cerebrovascular structure monitoring. *Sci. Rep.* 14:9245. doi: 10.1038/s41598-024-59529-y

Baz, R. A., Scheau, C., Niscoveanu, C., and Bordei, P. (2021). Morphometry of the entire internal carotid artery on CT angiography. *Medicina*. 57:832. doi: 10.3390/medicina57080832

Blankena, R., Kleinloog, R., Verweij, B. H., van Ooij, P., ten Haken, B., Luijten, P. R., et al. (2016). Thinner regions of intracranial Aneurysm Wall correlate with regions of higher wall shear stress: a 7T MRI study. *Am. J. Neuroradiol.* 37, 1310–1317. doi: 10.3174/ajnr.A4734

Brankov, J. G., Galatsanos, N. P., Yang, Y., and Wernick, M. N. (2003). Segmentation of dynamic PET or fMRI images based on a similarity metric. *IEEE Trans. Nucl. Sci.* 50, 1410–1414. doi: 10.1109/TNS.2003.817963

Caldeira, L., Kops, E. R., Yun, S. D., Silva, N., Mauler, J., Weirich, C., et al. (2019). The Jülich experience with simultaneous 3T MR-BrainPET: methods and technology. *IEEE Trans. Radiat. Plasma Med. Sci.* 3, 352–362. doi: 10.1109/TRPMS.2018.2863953

Caldeira, L. L., Yun, S. D., da Silva, N. A., Filss, C., and Shah, N. J. (2015). Conversion of the arterial input function using accelerated dual-contrast EPIK: A multi-modality MR-PET study. 23 ISMRM. Canada: Proc. Intl. Soc. Mag. Reson. Med.

Caldeira, L., Yun, S. D., da Silva, N., Filss, C., Scheins, J., Telmann, L., et al. (2015). Simultaneous acquisition of dynamic PET-MRI: arterial input function using DSC-MRI and [18F]-FET. *EJNMMI Phys.* 2:A70. doi: 10.1186/2197-7364-2-S1-A70

Catana, C. (2019). Development of dedicated brain PET imaging devices: recent advances and future perspectives. *J. Nucl. Med.* 60, 1044–1052. doi: 10.2967/jnumed.118.217901

Chavan, R., Hyman, G., Qureshi, Z., Jayakumar, N., Terrell, W., Wardius, M., et al. (2024). An end-to-end deep learning pipeline to derive blood input with partial volume corrections for automated parametric brain PET mapping. *Biomed Phys Eng Express.* 10:055028. doi: 10.1088/2057-1976/ad6a64

Chen, Z., Sforazzini, F., Baran, J., Close, T., Shah, N. J., and Egan, G. F. (2021). MR-PET head motion correction based on co-registration of multicontrast MR images. *Hum. Brain Mapp.* 42, 4081–4091. doi: 10.1002/hbm.24497

Chiu, S. C., Perucho, J. A. U., and Fang, Y. D. (2025). Motion correction of simultaneous brain PET/MR images based on tracer uptake characteristics. *EJNMMI Phys.* 12:75. doi: 10.1186/s40658-025-00789-6

Cosottini, M., Calzoni, T., Lazzarotti, G. A., Grigolini, A., Bosco, P., Cecchi, P., et al. (2024). Time-of-flight MRA of intracranial vessels at 7 T. *European Radiol. Experimental.* 8:68. doi: 10.1186/s41747-024-00463-z

Dahlbom, M., Schiepers, C., and Czernin, J. (2005). Comparison of noise equivalent count rates and image noise. *IEEE Trans. Nucl. Sci.* 52, 1386–1390. doi: 10.1109/TNS.2005.858176

da Silva, N. A., Caldeira, L., Herzog, H., Tellmann, L., Filss, C., Langen, K. J., et al. (2015). Automatic derivation of an MR-PET image-based input function for quantification of 18F-FET. *EJNMMI Phys.* 2:A27. doi: 10.1186/2197-7364-2-S1-A27

de Buck, M. H. S., Kent, J. L., Jezzard, P., and Hess, A. T. (2024). Head-and-neck multichannel B1+ mapping and RF shimming of the carotid arteries using a 7T parallel-transmit head coil. *Magn. Reson. Med.* 91, 190–204. doi: 10.1002/mrm.29845

De Cocker, L. J. L., Lindenholz, A., Zwanenburg, J. J. M., van der Kolk, A. G., Zwartbol, M., Luijten, P. R., et al. (2018). Clinical vascular imaging in the brain at 7T. *NeuroImage* 168, 452–458. doi: 10.1016/j.neuroimage.2016.11.044

de Salvi Souza, G., Mossel, P., Somsen, J. F., Providência, L., Bartels, A. L., Willemsen, A. T. M., et al. (2025). Evaluating image-derived input functions for cerebral [18F]MC225 PET studies. *Front. Nuclear Med.* 5:2025. doi: 10.3389/fnume.2025.1597902

Dimitrakopoulou-Strauss, A., Pan, L., and Sachpekidis, C. (2021). Kinetic modeling and parametric imaging with dynamic PET for oncological applications: general considerations, current clinical applications, and future perspectives. *Eur. J. Nucl. Med. Mol. Imaging* 48, 21–39. doi: 10.1007/s00259-020-04843-6

Driscoll, B., Shek, T., Vines, D., Sun, A., Jaffray, D., and Yeung, I. (2022). Phantom validation of a conservation of activity-based partial volume correction method for arterial input function in dynamic PET imaging. *Tomography.* 8, 842–857. doi: 10.3390/tomography8020069

Feinberg, D. A., Beckett, A. J. S., Vu, A. T., Stockmann, J., Huber, L., Ma, S., et al. (2023). Next-generation MRI scanner designed for ultra-high-resolution human brain imaging at 7 tesla. *Nat. Methods* 20, 2048–2057. doi: 10.1038/s41592-023-02068-7

Feng, J., Liu, X., Zhang, Z., Wu, Y., Li, Z., Zhang, Q., et al. (2022). Comparison of 7 T and 3 T vessel wall MRI for the evaluation of intracranial aneurysm wall. *Eur. Radiol.* 32, 2384–2392. doi: 10.1007/s00330-021-08331-9

Fink, G. R., and Schneider, F. (2007). "Von der Grundlagenforschung zum klinischen Einsatz in Diagnostik und Therapie" in Funktionelle MRT in Psychiatrie und Neurologie. eds. F. Schneider and G. R. Fink (Berlin, Heidelberg: Springer Berlin Heidelberg), 623–629.

Galovic, M., Erlandsson, K., Fryer, T. D., Hong, Y. T., Manavaki, R., Sari, H., et al. (2021). Validation of a combined image derived input function and venous sampling approach for the quantification of [(18)F]GE-179 PET binding in the brain. *NeuroImage* 237:118194. doi: 10.1016/j.neuroimage.2021.118194

Harteveld, A. A., De Cocker, L. J., Dieleman, N., van der Kolk, A. G., Zwanenburg, J. J., Robe, P. A., et al. (2015). High-resolution postcontrast time-of-flight MR angiography of intracranial perforators at 7.0 Tesla. *PLoS One* 10:e0121051. doi: 10.1371/journal.pone.0121051

Herzog, H., and Lerche, C. (2016). Advances in clinical PET/MRI instrumentation. *PET Clin.* 11, 95–103. doi: 10.1016/j.cpet.2015.09.001

Herzog, H., Langen, K. J., Weirich, C., Rota Kops, E., Kaffanke, J., Tellmann, L., et al. (2011). High resolution BrainPET combined with simultaneous MRI. *Nuklearmedizin* 50, 74–82. doi: 10.3413/Nukmed-0347-10-09

Hilgers, J, Anasovi, N, Scheins, J, Tellman, L, Lohmann, P, Filss, C, et al. (2025). Comparing estimated image derived input Fuinction based on priors and nnU-net segmentation: A pilot study. Turku, Finland: Turku PET Symposium. Poster Presentation.

Hoffman, E. J., Huang, S. C., and Phelps, M. E. (1979). Quantitation in positron emission computed tomography: 1. Effect of object size. *J. Comput. Assist. Tomogr.* 3, 299–308.

Hu, Y., Sanaat, A., Mathoux, G., Eliluane, P. A. T., Garibotto, V., and Zaidi, H. (2025). Deep learning-based triple-tracer brain PET scanning in a single session: a simulation study using clinical data. *NeuroImage* 313:121246. doi: 10.1016/j.neuroimage.2025.121246

Iida, H., Hori, Y., Ishida, K., Imabayashi, E., Matsuda, H., Takahashi, M., et al. (2013). Three-dimensional brain phantom containing bone and grey matter structures with a realistic head contour. *Ann. Nucl. Med.* 27, 25–36. doi: 10.1007/s12149-012-0655-7

Iwao, Y., Akamatsu, G., Tashima, H., Takahashi, M., and Yamaya, T. (2022). Brain PET motion correction using 3D face-shape model: the first clinical study. *Ann. Nucl. Med.* 36, 904–912. doi: 10.1007/s12149-022-01774-0

Jones, T., and Rabiner, E. A.Company PETRA (2012). The development, past achievements, and future directions of brain PET. *J. Cereb. Blood Flow Metab.* 32, 1426–1454. doi: 10.1038/jcbfm.2012.20

Kang, C.-K., Park, C.-A., Lee, D. S., Lee, Y.-B., Park, C.-W., Kim, Y.-B., et al. (2016). Velocity measurement of microvessels using phase-contrast magnetic resonance angiography at 7 tesla MRI. *Magn. Reson. Med.* 75, 1640–1646. doi: 10.1002/mrm.25600

Kang, H. G., Tashima, H., Wakizaka, H., Akamatsu, G., Iwao, Y., Toramatsu, C., et al. (2025). Development of an ultrasensitive small animal PET with 4-layer DOI detectors for sub-second dynamic rodent imaging. *Phys. Med. Biol.* 70:125014. doi: 10.1088/1361-6560/ade112

Kegeles, L. S., and Mann, J. J. (1997). In vivo imaging of neurotransmitter systems using radiolabeled receptor ligands. *Neuropsychopharmacology* 17, 293–307.

Kleinloog, R., Korkmaz, E., Zwanenburg, J. J. M., Kuijf, H. J., Visser, F., Blankena, R., et al. (2014). Visualization of the aneurysm wall: a 7.0-tesla magnetic resonance imaging study. *Neurosurgery* 75, 614–622. doi: 10.1227/NEU.0000000000000559

Kolb, A., Wehrl, H. F., Hofmann, M., Judenhofer, M. S., Eriksson, L., Ladebeck, R., et al. (2012). Technical performance evaluation of a human brain PET/MRI system. *Eur. Radiol.* 22, 1776–1788. doi: 10.1007/s00330-012-2415-4

Koning, W., de Rotte, A. A. J., Bluemink, J. J., van der Velden, T. A., Luijten, P. R., Klomp, D. W. J., et al. (2015). MRI of the carotid artery at 7 tesla: quantitative comparison with 3 tesla. *J. Magn. Reson. Imaging* 41, 773–780. doi: 10.1002/jmri.24601

Kuo, A. H., Nagpal, P., Ghoshhajra, B. B., and Hedgire, S. S. (2019). Vascular magnetic resonance angiography techniques. *Cardiovascular Diagnosis and Therapy.* 9, S28–S36. doi: 10.21037/cdt.2019.06.07

Lerche, CW, Niekämper, D, Scheins, JJ, Tellmann, L, Ridder, D, Kitten, Y, et al., editors. "First performance results of a UHF-MRI compatible BrainPET insert for neuroscience." *2023 IEEE nuclear science symposium, medical imaging conference and international symposium on room-temperature semiconductor detectors (NSS MIC RTSD)*; (2023) 4–11.

Lerche, C. W., Pietrzyk, U., and Lenz, M. (2018). "Positron emission tomography instrumentation" in Hybrid MR-PET imaging: Systems, methods and applications. ed. N. J. Shah (London: The Royal Society of Chemistry).

Liaw, C. Y., and Guvendiren, M. (2017). Current and emerging applications of 3D printing in medicine. *Biofabrication* 9:024102. doi: 10.1088/1758-5090/aa7279

Li, H., Badawi, R. D., Cherry, S. R., Fontaine, K., He, L., Henry, S., et al. (2024). Performance characteristics of the NeuroEXPLORER, a next-generation human brain PET/CT imager. *J. Nucl. Med.* 65:267767. doi: 10.2967/jnumed.124.267767

Liptrot, M., Adams, K. H., Martiny, L., Pinborg, L. H., Lonsdale, M. N., Olsen, N. V., et al. (2004). Cluster analysis in kinetic modelling of the brain: a noninvasive alternative to arterial sampling. *NeuroImage* 21, 483–493. doi: 10.1016/j.neuroimage.2003.09.058

Lopresti, B. J., Klunk, W. E., Mathis, C. A., Hoge, J. A., Ziolko, S. K., Lu, X., et al. (2005). Simplified quantification of Pittsburgh Compound B amyloid imaging PET studies: a comparative analysis. *J Nucl Med.* 46, 1959–1972.

Ma, B., Gaens, M., Caldeira, L., Bert, J., Lohmann, P., Tellmann, L., et al. (2020). Scatter correction based on GPU-accelerated full Monte Carlo simulation for brain PET/MRI. *IEEE Trans. Med. Imaging* 39, 140–151. doi: 10.1109/TMI.2019.2921872

Maccioni, L., Michelle, C. M., Brusaferri, L., Silvestri, E., Bertoldo, A., Schubert, J. J., et al. (2024). A blood-free modeling approach for the quantification of the blood-to-brain tracer exchange in TSPO PET imaging. *Front. Neurosci.* 18:2024. doi: 10.3389/fnins.2024.1395769

Maroy, R., Boisgard, R., Comtat, C., Frouin, V., Cathier, P., Duchesnay, E., et al. (2008). Segmentation of rodent whole-body dynamic PET images: an unsupervised method based on voxel dynamics. *IEEE Trans. Med. Imaging* 27, 342–354. doi: 10.1109/TMI.2007.905106

Mauler, J., Heinzel, A., Matusch, A., Herzog, H., Neuner, I., Scheins, J., et al. (2020). Bolus infusion scheme for the adjustment of steady state [(11)C]flumazenil levels in the grey matter and in the blood plasma for neuroreceptor imaging. *NeuroImage* 221:117160. doi: 10.1016/j.neuroimage.2020.117160

Mauler, J., Lohmann, P., Maudsley, A. A., Sheriff, S., Hoevels, M., Meissner, A. K., et al. (2024). Diagnostic accuracy of MR spectroscopic imaging and (18)F-FET PET for identifying glioma: a biopsy-controlled hybrid PET/MRI study. *J. Nucl. Med.* 65, 16–21. doi: 10.2967/jnumed.123.265868

Montgomery, A. J., Thielemans, K., Mehta, M. A., Turkheimer, F., Mustafovic, S., and Grasby, P. M. (2006). Correction of head movement on PET studies: comparison of methods (Online ISSN 2159-662X). *J. Nucl. Med.* 47:1936.

Naganawa, M., Kimura, Y., Ishii, K., Oda, K., Ishiwata, K., and Matani, A. (2005). Extraction of a plasma time-activity curve from dynamic brain PET images based on independent component analysis. *IEEE Trans. Biomed. Eng.* 52, 201–210. doi: 10.1109/TBME.2004.840193

Niekämper, D., Scheins, J. J., Schug, D., Liu, Q., Shah, N. J., and Lerche, C. (2025). Timing calibration and coincidence time resolution of the BrainPET-7T insert. *TechRxiv.*, 1–8. doi: 10.36227/techrxiv.176114259.94036940/v1

Osuafor, C. N., Rua, C., Mackinnon, A. D., Egle, M., Benjamin, P., Tozer, D. J., et al. (2022). Visualisation of lenticulostriate arteries using contrast-enhanced time-of-flight magnetic resonance angiography at 7 tesla. *Sci. Rep.* 12:20306. doi: 10.1038/s41598-022-24832-z

Park, C.-A., Kang, C.-K., Kim, Y.-B., and Cho, Z.-H. (2018). Advances in MR angiography with 7T MRI: from microvascular imaging to functional angiography. *NeuroImage* 168, 269–278. doi: 10.1016/j.neuroimage.2017.01.019

Pfaehler, E., Niekämper, D., Scheins, J., Shah, N. J., and Lerche, C. W. (2024). ML-EM based dual tracer PET image reconstruction with inclusion of prompt gamma attenuation. *Phys. Med. Biol.* 70, 1–16. doi: 10.1088/1361-6560/ad9660

Rajkumar, R., Farrher, E., Mauler, J., Sripad, P., Régio Brambilla, C., Rota Kops, E., et al. (2021). Comparison of EEG microstates with resting state fMRI and FDG-PET measures in the default mode network via simultaneously recorded trimodal (PET/MR/EEG) data. *Hum. Brain Mapp.* 42, 4122–4133. doi: 10.1002/hbm.24429

Ramnarine, K. V., Nassiri, D. K., Hoskins, P. R., and Lubbers, J. (1998). Validation of a new blood-mimicking fluid for use in Doppler flow test objects. *Ultrasound Med. Biol.* 24, 451–459.

Régio Brambilla, C., Veselinović, T., Rajkumar, R., Mauler, J., Matusch, A., Ruch, A., et al. (2022). mGluR5 binding changes during a mismatch negativity task in a multimodal protocol with [11C]ABP688 PET/MR-EEG. *Transl. Psychiatry* 12:6. doi: 10.1038/s41398-021-01763-3

Ronneberger, O., Fischer, P., and Brox, T. (2015). "U-net: convolutional networks for biomedical image segmentation" in Medical image computing and computer-assisted intervention – MICCAI 2015. eds. N. Navab, J. Hornegger, W. M. Wells and A. F. Frangi (Cham: Springer International Publishing).

Salvi de Souza, G., Mossel, P., Somsen, J. F., Providência, L., Bartels, A. L., Willemsen, A. T. M., et al. (2025). Evaluating image-derived input functions for cerebral [18F]MC225 PET studies. *Frontiers in Nuclear Medicine.* 5:2025.

Scheins, J. J., Herzog, H., and Shah, N. J. (2011). Fully-3D PET image reconstruction using scanner-independent, adaptive projection data and highly rotation-symmetric voxel assemblies. *IEEE Trans. Med. Imaging* 30, 879–892. doi: 10.1109/TMI.2011.2109732

Scheins, J. J., Lenz, M., Pietrzyk, U., Shah, N. J., and Lerche, C. (2021). High-throughput, accurate Monte Carlo simulation on CPU hardware for PET applications. *Phys. Med. Biol.* 66, 1–20. doi: 10.1088/1361-6560/ac1ca0

Scheins, J. J., Vahedipour, K., Pietrzyk, U., and Shah, N. J. (2015). High performance volume-of-intersection projectors for 3D-PET image reconstruction based on polar symmetries and SIMD vectorisation. *Phys. Med. Biol.* 60, 9349–9375. doi: 10.1088/0031-9155/60/24/9349

Schlemmer, H. P., Pichler, B. J., Schmand, M., Burbar, Z., Michel, C., Ladebeck, R., et al. (2008). Simultaneous MR/PET imaging of the human brain: feasibility study. *Radiology* 248, 1028–1035. doi: 10.1148/radiol.2483071927

Schmitter, S., Adriany, G., Waks, M., Moeller, S., Aristova, M., Vali, A., et al. (2020). Bilateral multiband 4D flow MRI of the carotid arteries at 7T. *Magn. Reson. Med.* 84, 1947–1960. doi: 10.1002/mrm.28256

Seginer, A., Niry, D., Furman-Haran, E., Kolb, H., and Schmidt, R. (2024). Reducing blood flow pulsation artifacts in 3D time-of-flight angiography by locally scrambling the order of the acquisition at 3 T and 7 T. *Magn. Reson. Med.* 92, 2081–2090. doi: 10.1002/mrm.30196

Silvestri, E., Volpi, T., Bettinelli, A., De Francisci, M., Jones, J., Corbetta, M., et al. (2022). Image-derived input function in brain [(18)F]FDG PET data: Which alternatives to the carotid siphons? *Annu Int Conf IEEE Eng med biol Soc* 2022, 243–246. doi: 10.1109/EMBC48229.2022.9871200

Spangler-Bickell, M. G., Hurley, S. A., Pirasteh, A., Perlman, S. B., Deller, T., and McMillan, A. B. (2022). Evaluation of data-driven rigid motion correction in clinical brain PET imaging. *J. Nucl. Med.* 63, 1604–1610. doi: 10.2967/jnumed.121.263309

Springer, E., Dymerska, B., Cardoso, P. L., Robinson, S. D., Weisstanner, C., Wiest, R., et al. (2016). Comparison of routine brain imaging at 3 T and 7 T. *Investig. Radiol.* 51, 469–482. doi: 10.1097/RLI.0000000000000256

Sundar, L. K., Muzik, O., Rischka, L., Hahn, A., Rausch, I., Lanzenberger, R., et al. (2019). Towards quantitative [18F]FDG-PET/MRI of the brain: automated MR-driven calculation of an image-derived input function for the non-invasive determination of cerebral glucose metabolic rates. *J. Cereb. Blood Flow Metab.* 39, 1516–1530. doi: 10.1177/0271678X18776820

Ullisch, M. G., Scheins, J. J., Weirich, C., Rota Kops, E., Celik, A., Tellmann, L., et al. (2012). MR-based PET motion correction procedure for simultaneous MR-PET neuroimaging of human brain. *PLoS One* 7:e48149. doi: 10.1371/journal.pone.0048149

van der Kolk, A. G., Hendrikse, J., Brundel, M., Biessels, G. J., Smit, E. J., Visser, F., et al. (2013). Multi-sequence whole-brain intracranial vessel wall imaging at 7.0 tesla. *Eur. Radiol.* 23, 2996–3004. doi: 10.1007/s00330-013-2905-z

van der Weijden, C. W. J., Mossel, P., Bartels, A. L., Dierckx, R., Luurtsema, G., Lammertsma, A. A., et al. (2023). Non-invasive kinetic modelling approaches for quantitative analysis of brain PET studies. *Eur. J. Nucl. Med. Mol. Imaging* 50, 1636–1650. doi: 10.1007/s00259-022-06057-4

Vestergaard, M. B., Calvo, O. P., Hansen, A. E., Rosenbaum, S., Larsson, H. B. W., Henriksen, O. M., et al. (2021). Validation of kinetic modeling of [15O]H2O PET using an image derived input function on hybrid PET/MRI. *NeuroImage* 233:117950. doi: 10.1016/j.neuroimage.2021.117950

Volpi, T., Maccioni, L., Colpo, M., Debiasi, G., Capotosti, A., Ciceri, T., et al. (2023). An update on the use of image-derived input functions for human PET studies: new hopes or old illusions? *EJNMMI Res.* 13:97. doi: 10.1186/s13550-023-01050-w

Volpi, T., Zeng, T., Khattar, N., Toyonaga, T., Martins, S., Mulnix, T., et al. editors. "Image-derived input functions on an ultra-high performance brain PET scanner: minimizing the carotid partial volume effect." *2024 IEEE nuclear science symposium (NSS), medical imaging conference (MIC) and room temperature semiconductor detector conference (RTSD)*; (2024).

Volpi, T., Gallezot, J-D., Henry, S., Dias, M., Khattar, N., Toyonaga, T., et al. (2025). Carotid Artery Image-Derived Blood Time–Activity Curves on the NeuroEXPLORER: Initial Multitracer Validation Against Arterial Sampling. *Journal of Nuclear Medicine*. 2025:jnumed.125.270414.

von Morze, C., Xu, D., Purcell, D. D., Hess, C. P., Mukherjee, P., Saloner, D., et al. (2007). Intracranial time-of-flight MR angiography at 7T with comparison to 3T. *J. Magn. Reson. Imaging* 26, 900–904. doi: 10.1002/jmri.21097

Wang, J., Bermudez, D., Chen, W., Durgavarjhula, D., Randell, C., Uyanik, M., et al. (2024). Motion-correction strategies for enhancing whole-body PET imaging. *Front. Nuclear Med.* 4:2024. doi: 10.3389/fnume.2024.1257880

Won, J. Y., Park, H., Lee, S., Son, J. W., Chung, Y., Ko, G. B., et al. (2021). Development and initial results of a brain PET insert for simultaneous 7-tesla PET/MRI using an FPGA-only signal digitization method. *IEEE Trans. Med. Imaging* 40, 1579–1590. doi: 10.1109/TMI.2021.3062066

Yun, S. D., Reske, M., Vahedipour, K., Warbrick, T., and Shah, N. J. (2013). Parallel imaging acceleration of EPIK for reduced image distortions in fMRI. *NeuroImage* 73, 135–143. doi: 10.1016/j.neuroimage.2013.01.070

Zanotti-Fregonara, P., Fadaili, E. M., Maroy, R., Comtat, C., Souloumiac, A., Jan, S., et al. (2009). Comparison of eight methods for the estimation of the image-derived input function in dynamic [18F]-FDG PET human brain studies. *J. Cereb. Blood Flow Metab.* 29, 1825–1835. doi: 10.1038/jcbfm.2009.93

Zeng, T., Lu, Y., Jiang, W., Zheng, J., Zhang, J., Gravel, P., et al. (2023). Markerless head motion tracking and event-by-event correction in brain PET. *Phys. Med. Biol.* 68:245019. doi: 10.1088/1361-6560/ad0e37

Zhang, K., Herzog, H., Mauler, J., Filss, C., Okell, T. W., Kops, E. R., et al. (2014). Comparison of cerebral blood flow acquired by simultaneous [15O]water positron emission tomography and arterial spin labeling magnetic resonance imaging. *J. Cereb. Blood Flow Metab.* 34, 1373–1380. doi: 10.1038/jcbfm.2014.92

Zhu, C., Haraldsson, H., Tian, B., Meisel, K., Ko, N., Lawton, M., et al. (2016). High resolution imaging of the intracranial vessel wall at 3 and 7 T using 3D fast spin echo MRI. *MAGMA* 29, 559–570. doi: 10.1007/s10334-016-0531-x

Zhu, C., Tian, B., Chen, L., Eisenmenger, L., Raithel, E., Forman, C., et al. (2018). Accelerated whole brain intracranial vessel wall imaging using black blood fast spin echo with compressed sensing (CS-SPACE). *MAGMA* 31, 457–467. doi: 10.1007/s10334-017-0667-3

Zhu, Y., Chen, L., Lu, W., Gong, Y., and Wang, X. (2022). The application of the nnU-net-based automatic segmentation model in assisting carotid artery stenosis and carotid atherosclerotic plaque evaluation. *Front. Physiol.* 13:2022. doi: 10.3389/fphys.2022.1057800